

Article

Occurrence Form of Potassium Vapor in Sinter and Its Effect on Reduction Degradation Indexes

Jiantao Ju ^{1,2}, Huayong Wang ^{1,2}, Xiangdong Xing ^{1,2}, Manbo Liu ^{1,2,*}, Guiqing Zhao ³ and Xintai Jiang ³¹ School of Metallurgical Engineering, Xi'an University of Architecture and Technology, Xi'an 710055, China² Research Center of Metallurgical Engineering Technology of Shaanxi Province, Xi'an 710055, China³ Technical Center of Jiuquan Iron and Steel (Group) Co., Ltd., Jiayuguan 735100, China

* Correspondence: liumanbo@xauat.edu.cn

Abstract: In this study, potassium vapor was prepared by using potassium carbonate (K_2CO_3) and activated carbon (C) reagents to simulate the actual situation of adsorbing potassium vapor from the sinter in the blast furnace. The potassium-rich sinter was characterized by X-ray diffraction (XRD), flame atomic absorption spectrometry (FAAS), and scanning electron microscopy (SEM-EDS). The effects of potassium vapor content on the enrichment ratio, adsorption rate, and low-temperature reduction degradation index ($RDI_{+3.15mm}$) of sinter have been studied. The results show that with the increase of potassium vapor content, the enrichment ratio of potassium in the sinter increases, and the adsorption rate of potassium in the sinter increases first and then decreases, which was opposite to the trend of the low-temperature reductive degradation index of the sinter. When the potassium vapor content was increased by 50 times, the enrichment ratio and low-temperature reduction powder of the sinter are the highest, which were 2576% and 85.3%, respectively, and the adsorption rate of the sinter was the lowest, which is 51.5%. Meanwhile, potassium vapor changes from physical adsorption K_2CO_3 to chemical adsorption $KFeO_2$ as the potassium vapor content increases. In addition, the transformation of the occurrence form of potassium vapor in the sinter during the rising process has also been clarified.

Keywords: sinter; potassium vapor; enrichment; reduction degradation indexes; occurrence form

Citation: Ju, J.; Wang, H.; Xing, X.; Liu, M.; Zhao, G.; Jiang, X.

Occurrence Form of Potassium Vapor in Sinter and Its Effect on Reduction Degradation Indexes. *Metals* **2023**, *13*, 1010. <https://doi.org/10.3390/met13061010>

Academic Editor: Alexander McLean

Received: 14 April 2023

Revised: 17 May 2023

Accepted: 19 May 2023

Published: 24 May 2023



Copyright: © 2023 by the authors. Licensee MDPI, Basel, Switzerland. This article is an open access article distributed under the terms and conditions of the Creative Commons Attribution (CC BY) license (<https://creativecommons.org/licenses/by/4.0/>).

1. Introduction

With the rapid development of steel production, the price of high-quality iron ore continues to rise. To combat the problem, numerous iron and steel companies opt to utilize low-grade ore in large quantities and supplement it with a significant amount of ferrous metallurgical solid waste in the raw materials [1,2]. Iron-bearing low-grade ores and metallurgical wastes are known for containing high levels of harmful elements, including alkali metals such as K and Na, which will increase the alkali loads on blast furnaces [3,4]. Additionally, alkali metals are cyclically enriched in the form of alkali vapor within the blast furnace [5,6]. During the circulation process, alkali steam will inevitably contact with the metallurgical raw material and furnace lining of the blast furnace, which will have negative effects on production [7,8]. For instance, it will catalyze the gasification and dissolution loss [9,10], and both pellet expansion [11,12] and the sintering reduction pulverization index may increase [13], and destroy the corrosion-resistant materials in blast furnaces [14,15]. In the traditional ironmaking process, sinter is one of the main raw materials of blast furnace smelting. China, Japan, and South Korea account for 75–80% of blast furnace ironmaking raw materials [16,17]. The quality of the sinter plays a decisive role in the output, energy consumption, pig iron quality, and life of the blast furnace. Therefore, it is necessary to study the influence of alkali metals on sinter.

The present research mainly focuses on the influence of alkali metals on sinter properties [18–22]. M. Bahgat et al. [18] studied the effect of K_2O on the oxidation and reduction

behavior and found that when alkali metals were present in Fe_2O_3 , the abnormal expansion would occur in the reduction process, which was caused by crystal cracking at the initial reduction stage and the formation of fibrous iron or carbon deposition on reduced iron. Zhang et al. [19] explored the influence rule of alkali metals on sinter strength by adding dust ash to sintering ingredients. With the dust ash content increasing from 0% to 3.23%, the alkali metal content of the sinter increased from 0.15% to 0.25%, and the drum strength of the sinter decreased from 81.07% to 75.47%. Yan et al. [20] found that with the increase of enriched potassium content in the sinter, the reduction degree of the sinter increased from 73.1% to 81.3%. The reduction degradation index $RDI_{+3.15\text{mm}}$ first decreased and then gradually increased, while the softening starting temperature of the sinter with rich potassium decreased, and the soft melting temperature range widened. Kang et al. [21] found that with the increase of alkali metals and zinc in iron ore, the $RDI_{+6.3\text{mm}}$ and $RDI_{+3.15\text{mm}}$ indexes of sinter and pellets decreased slightly, while the $RDI_{-0.5\text{mm}}$ indexes increased slightly. Spraying CaCl_2 solution on the surface of the sinter could significantly improve the low-temperature reduction degradation index of the sinter. Wang et al. [22] studied the reaction behavior of alkali metal vapor with sinter and found that most K and Na vapor evaporated to the surface of sinter and reacted with sinter to form a “light enriched layer” with K, Na compounds, Fe_2O_3 , and calcium ferrite as the main phases. As the pore is blocked, a “deep enrichment layer” is formed outside the “light enrichment layer”. The main phase of the “deep enrichment layer” is potassium oxide and sodium oxide, and the content of sodium oxide is higher than that of potassium oxide. Although previous studies have confirmed the adverse effects of alkali metal on the performance of sinter, considering the high content of alkali metal steam in the blast furnace and the characteristic that rises with the gas, the influence of alkali metal steam content on the performance of the sinter and the variation rule of occurrence form in the sinter should be studied more systematically.

In this work, the potassium vapor enrichment experiment was carried out in the high-temperature vertical resistance furnace by simulating the actual situation of potassium cyclic enrichment in the blast furnace. The effects of potassium vapor content on sinter enrichment ratio, adsorption rate, and low-temperature reduction degradation performance have been studied. The effects of potassium vapor content on phase composition, microstructure, and element distribution of sintered minerals were investigated. At the same time, the variation rule of the occurrence form of potassium vapor in the sinter mine with the gas rises has been clarified, which provides a theoretical basis for further study.

2. Materials and Methods

2.1. Raw Materials

The sinter used for the experiment was obtained from the blast furnace production site of a steel mill, and its composition is provided in Table 1. The alkalinity of the sinter was 1.93, and the content of K was 0.28 wt. %. After crushed using a jaw crusher, only the sinter with a particle size of 10.0–12.5 mm was selected for the experiment. Before the experiment, the sintered samples were dried in an oven at 120 °C until they were no longer losing weight.

Table 1. Chemical composition of sinter sample (wt. %).

TFe	FeO	CaO	SiO ₂	Al ₂ O ₃	MgO	ZnO	K	Na ₂ O
49.95	9.25	14.28	7.41	1.84	2.69	0.22	0.28	0.32

The analytical reagent powder used in this study was obtained from the controlling chemical reagent co., LTD. It includes K_2CO_3 with a purity level of $\geq 99.0\%$ and analytically pure activated carbon with a burned residue of $\leq 2.0\%$. Potassium vapor was generated through the reduction of K_2CO_3 using activated carbon.

Since the Gibbs free energy of the reduction reaction was negative, the following chemical reaction could be carried out at 1200 °C and generate standard potassium vapor. During the rising process, the sintered ore sample adsorbed potassium vapor and a kind of potassium-rich sintered ore sample was obtained. The reaction is shown in Equation (1):



2.2. The Alkali Metal Adsorption of Sinter

Before the experiment, the temperature distribution of the high-temperature vertical resistance furnace was measured: the resistance furnace was first heated to 1200 °C, and the constant temperature was set. The k-type thermocouple was used to determine the isothermal range of the resistance furnace. When the thermocouple reading was 1200 °C, it was marked as “0 cm” and the thermocouple was lifted upward. When the thermocouple temperature was 1000 °C, 800 °C, 600 °C, 500 °C, 400 °C, and no longer changing, the height of each temperature position was recorded.

The gas composition ($\text{N}_2 + \text{CO} + \text{CO}_2$) in each temperature section of the blast furnace should be determined first. The content of N_2 in each temperature section of the blast furnace changes little, generally about 60–70%. In this paper, the content of N_2 in each temperature section was selected as 60%. As shown in Figure 1, the gas atmosphere ($\text{CO} + \text{CO}_2$) at each temperature segment was fitted [23–26], and the gas composition ($\text{N}_2 + \text{CO} + \text{CO}_2$) at each temperature of the blast furnace was fitted, as shown in Table 2.

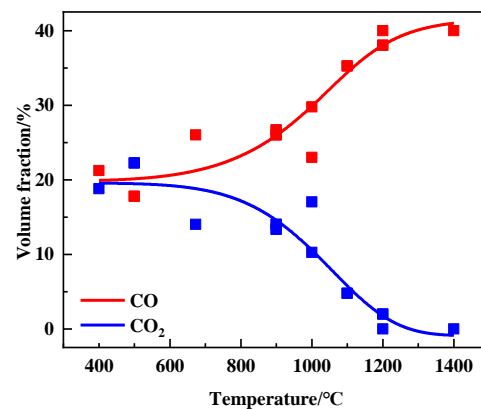


Figure 1. Composition of blast furnace gas ($\text{CO} + \text{CO}_2$).

Table 2. Design of blast furnace gas.

Temperature/°C	$\text{CO}_2/\text{mL}\cdot\text{min}^{-1}$	$\text{CO}/\text{mL}\cdot\text{min}^{-1}$	$\text{N}_2/\text{mL}\cdot\text{min}^{-1}$
400	200	200	600
500	200	200	600
600	190	210	600
800	170	230	600
1000	100	300	600
1200	20	380	600

A series of adsorption experiments were carried out in a high-temperature vertical resistance furnace, in which a basket containing sinter samples was placed at the height of the experiment temperature [27–29]. K_2CO_3 was fully mixed with activated carbon and then loaded into the corundum crucible placed in the position of “0”. Next, 1 L/min nitrogen (N_2) was injected as the protective gas and the sample was heated at a rate of 10 °C/min to 1200 °C, and then the mixture gas ($\text{CO}_2 + \text{CO} + \text{N}_2$) with a flow rate of 1 L/min was kept constant for 90 min (10 min was the thermal stability time, 80 min was

the experiment time). After the experiment, the gas was switched to 1 L/min N_2 and cooled to room temperature naturally. The experimental device is shown in Figure 2.

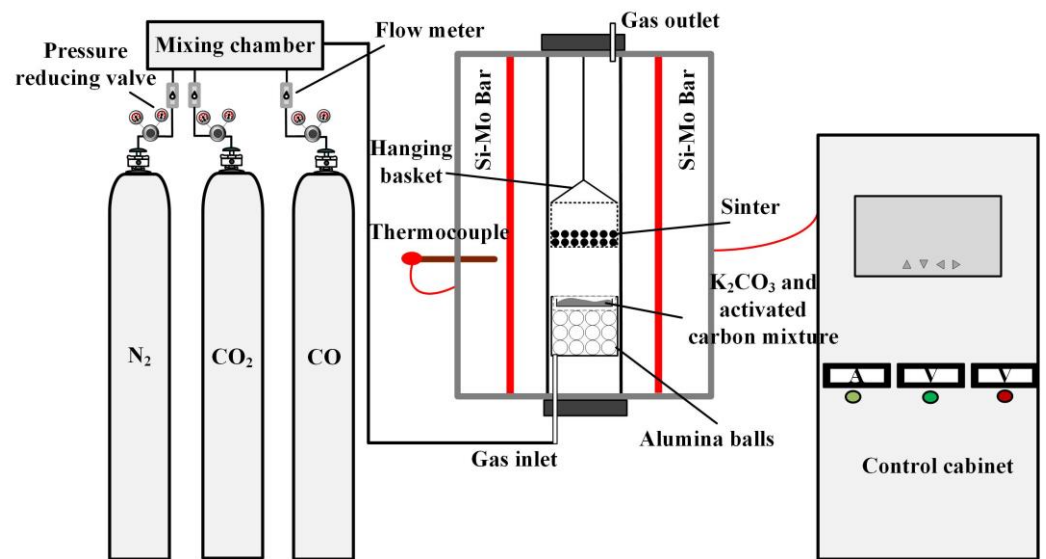


Figure 2. Schematic diagram of potassium-rich experimental apparatus.

According to the statistics of the blast furnace site, the content of potassium vapor in the blast furnace belly is up to 50 times the potassium load [26]. Therefore, potassium vapor was selected as 0, 10, 20, 30, 40, and 50 times the basal potassium load in the experiment. The basal potassium load was determined based on the 0.28% K content in the sinter and the sinter quality. In order to ensure the complete reaction of K_2CO_3 , an additional 50% activated carbon was added. The mass ratio of K_2CO_3 to sinter was set as 0, 0.05, 0.10, 0.15, 0.20, and 0.25, respectively. The mass ratio of activated carbon to K_2CO_3 was fixed at 0.26. Experimental material is shown in Table 3.

Table 3. Experimental material.

Sample	Sinter Mass/g	K/g	K_2CO_3 /g	Activated Carbon/g
K-0	57.1	-	-	-
K-10	58.2	1.63	2.88	0.75
K-20	60.1	3.37	5.95	1.55
K-30	60.3	5.07	8.96	2.34
K-40	56.1	6.28	11.12	2.90
K-50	59.3	8.30	14.69	3.83
L-400	58.5	6.55	11.59	3.02
L-600	59	6.61	11.69	3.05
L-800	58.4	6.54	11.57	3.02
L-1000	56.4	6.32	11.18	2.92
L-1200	54.7	6.13	10.84	2.83

2.3. Characterization Methods

The sinter was finely ground to less than 200 mesh using an agate mortar for subsequent analysis by X-ray diffractometry (XRD), flame atomic absorption spectrometry (FAAS), specific surface area, and pore size. The sinter samples were inserted into epoxy resin and then polished successively (400, 600, 800, 1200, and 2000 CW) for scanning electron microscope and energy dispersive spectroscopy (SEM-EDS) analysis. The sintered samples were finally put into the drum for pulverization performance (RDI) measuring.

The determination of potassium content in sintered ore was carried out according to GB/T 6730.49-2017 [30]. The United States thermoelectric iCE 3300 AA System atomic

absorption spectrometer was used to determine the content of potassium in sinter, and the enrichment ratio and adsorption rate of K were calculated.

The enrichment ratio and adsorption rate of K are expressed by X_a and X_e , respectively, which are defined as follows:

$$X_a = \frac{W_2 - W_1}{W_1} \times 100\% \quad (2)$$

$$X_e = \frac{W_2 - W_1}{X_o} \times 100\% \quad (3)$$

$$X_o = Y/Z \times 100\% \quad (4)$$

where W_2 and W_1 are the mass of K in the potassium-rich sinter and the original sinter, respectively, %. X_o is the potassium content adsorbed by theoretical sinter, %; Y is the content of potassium vapor generated by the reaction of K_2CO_3 and activated carbon, g; and Z is the mass of the sinter, g.

The specific surface area and pore volume of the sinter before and after potassium enrichment were determined by BET (JW-BK222, China Jingwei Science and Technology Company, Beijing, China). The degassing temperature was 200 °C and the degassing time was 240 min. The adsorbent was high-purity N_2 , and the working temperature was 77.3 K. D8 ADVANCE XRD (Bruker, Billerica, MA, USA) was used for XRD analysis, Cu Ka was used as a radiation source (40 kV, 400 mA), and the scanning speed was 1°/min, whose scanning range was 20–90°. The potassium-rich sinter was embedded in epoxy resin and polished. SEM imaging and energy spectrum analysis were performed by SEM-EDS (VEGA 3 XMU/XMH, Tescan, Brno, Czech Republic).

The low-temperature comminution performance of the sinter was determined according to GB/T 13241-2017 [31]. The low-temperature reduction degradation indexes of the sinter were $RDI_{+6.3mm}$, $RDI_{+3.15mm}$, and $RDI_{-0.5mm}$. According to Equations (5)–(7):

$$RDI_{+6.3mm} = \frac{m_{+6.3}}{m_1} \times 100\% \quad (5)$$

$$RDI_{+3.15mm} = \frac{m_{+3.15}}{m_1} \times 100\% \quad (6)$$

$$RDI_{-0.5mm} = \frac{m_{-0.5}}{m_1} \times 100\% \quad (7)$$

where $m_{+6.3}$ is the mass of sinter with a size of 6.30 mm after drum rotation, g; $m_{+3.15}$ is the mass of sinter with a particle size of 3.15–6.3 mm after drum rotation, g; $m_{-0.5}$ refers to the mass of sinter with particle size less than 0.5 mm after drum rotation, g; and m_1 is the original mass of sinter, g.

3. Results and Discussion

3.1. Effect of Potassium Vapor on Potassium Enrichment Ratio and Adsorption Rate of Sinter

A corundum crucible containing different K_2CO_3 contents and activated carbon was placed at 1200 °C (position “0”). The basket containing sintered ore was suspended at the corresponding position at 500 °C and heated for 90 min at 1200 °C. Table 4 shows the change in K content of the sinter after the potassium-rich experiment, while Figure 3 displays the specific surface area and pore volume of the sinter with varying content of potassium vapor.

As can be seen from Table 4, the enrichment ratio was used to characterize the change of K content during the experiment, and the adsorption rate was used to characterize the adsorption capacity of the sinter. Potassium can be effectively enriched in the sinter. With the increase of potassium vapor, the enrichment ratio of the sinter gradually increases. When the potassium vapor content increased from 10 to 50 times higher, the enrichment

ratio of potassium in the sinter gradually increased from 538% to 2576%. With the increase of potassium vapor, the enrichment ratio of the sinter gradually increased, and the adsorption rate capacity of the sinter increased first and then decreased gradually. When the content of potassium vapor was 50 times higher, the adsorption rate of potassium was the highest, which was 51.5%.

Table 4. Potassium content in sinter after potassium enrichment experiment.

Sample	Original Content/wt%	Enrichment Content/wt%	Enrichment Ratio/%	Adsorption Rate/%
K-0	0.28	0.26	-	-
K-10	0.28	1.79	538	53.8
K-20	0.28	4.18	1391	69.5
K-30	0.28	6.42	2191	73.0
K-40	0.28	6.83	2338	58.5
K-50	0.28	7.49	2576	51.5

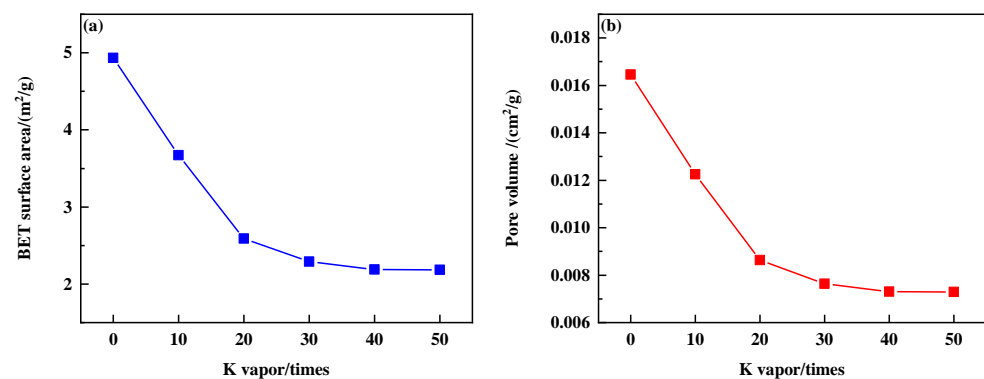


Figure 3. Relationship between water vapor content and specific surface area and pore volume at different temperatures. (a) BET surface area; (b) pore volume.

As can be seen from Figure 3, the specific surface area of the sinter is shown in Figure 3a and the pore volume in Figure 3b shows similar variation rules. With the increase of potassium vapor content, the specific surface area and pore volume of the sinter decreased gradually. When potassium vapor content exceeded 20 times higher, the specific surface area and pore volume of the sinter gradually became stable.

According to the analysis in Table 4 and Figure 3, the enrichment ratio of sinter gradually increases with the increase of potassium vapor content, because the porous structure of sinter facilitates it generating potassium vapor to enter the sinter. Meanwhile, potassium has high chemical activity and will react with the sinter to improve the potassium content in the sinter, resulting in the reduction of specific surface area and pore volume. With the increase of potassium vapor content, the adsorption rate of sinter increases and decreases successively. When the content of potassium vapor is low, the sinter can adsorb potassium vapor, and the adsorption rate is higher. When the potassium vapor content is too high, the pores and cracks of the sinter are blocked due to the increase of the potassium content on the surface of the sinter. The further reaction between the potassium vapor and the sinter is hindered, and the adsorption capacity of the sinter for potassium is gradually saturated. Therefore, the specific surface area and pore volume of sinter gradually become stable, and the adsorption of potassium increases and decreases successively.

3.2. Effect of Potassium Vapor on Sinter Reduction Chalking Index

The sinter samples with rich potassium content were put into a drum with an inner diameter of 130 mm and an inner length of 200 mm for 10 min at the speed of 30 r/min. Then, the sinter samples were screened with 6.30, 3.15, and 0.50 mm square holes. The weight obtained from sinter with different particles (>6.30, 3.15–6.30, 0.50–3.15, and <0.50 mm)

was measured, and the results are shown in Table 5. The effect of potassium content on the pulverizing property of the sinter is shown in Figure 4.

Table 5. Comparison of sinter drum quality with the different potassium content.

Sample	Drum Mass/g			
	$m_{+6.3\text{mm}}$	$m_{3.15-6.3\text{mm}}$	$m_{0.5-3.15\text{mm}}$	$m_{-0.5\text{mm}}$
K-0	41.6	0.5	1.4	9.1
K-10	39.5	1.6	1.8	11.2
K-20	37.8	2.8	4.9	10.8
K-30	43.8	3.5	5.9	11.6
K-40	40.9	5.9	6.3	9.0
K-50	45.3	5.3	8.7	6.8

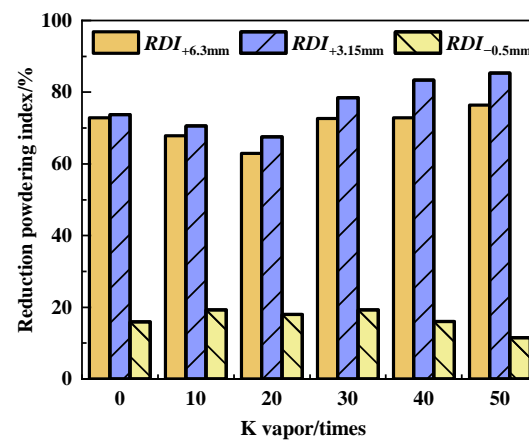


Figure 4. Effect of potassium content on pulverizing property of sinter.

Figure 4 shows that $RDI_{+6.3\text{mm}}$, $RDI_{+3.15\text{mm}}$, and $RDI_{-0.5\text{mm}}$ of unenriched potassium steam sinter are 72.85%, 73.73%, and 15.94%, respectively. When the content of potassium vapor increased from 10 to 20 times higher, the $RDI_{+3.15\text{mm}}$ of sinter decreased gradually. When the potassium vapor content is 10 times higher, the $RDI_{+3.15\text{mm}}$ reaches the minimum value of 67.55%. As the potassium vapor content continued to increase, the $RDI_{+3.15\text{mm}}$ gradually increased. When the potassium vapor content was 50 times higher, the $RDI_{+3.15\text{mm}}$ reached the maximum value of 85.33%.

This indicates that the enrichment of potassium vapor reduces the strength of the sinter, promotes the pulverization of the sinter, and reduces the $RDI_{+3.15\text{mm}}$ of the sinter, because potassium is favorable to enter the lattice of Fe_xO in the reduction process, and potassium has a large ionic radius, so it is difficult to diffuse evenly in the tightly packed crystals of Fe_xO . Therefore, stress will appear at the junction of the new phase and the parent phase. When the stress accumulates to a certain amount, the new phase will crack along the interface or weak direction of the grain, resulting in distortion of the lattice on the surface of Fe_xO and local reduction degradation. However, with the further increase of potassium content, $RDI_{+3.15\text{mm}}$ gradually increased. Because potassium existing in the surface pores of the sinter can reduce the contact between the sinter and reduction gas to some extent, and it diffuses more evenly in Fe_xO crystal, the effect of potassium on pulverization damage in the reduction process of sinter is relatively weakened, and the $RDI_{+3.15\text{mm}}$ index of sinter is increased.

3.3. Occurrence Form of Potassium in Sinter Mine

3.3.1. Phase Analysis of Potassium-Rich Sinter

X-ray diffraction (XRD) was used to analyze the influence of potassium vapor on the phase evolution of potassium-rich sinter, as shown in Figure 5.

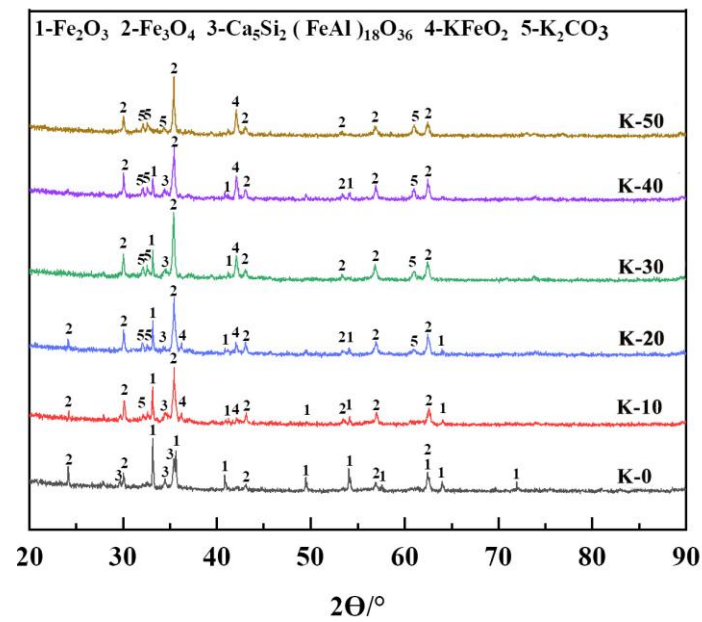


Figure 5. XRD pattern of potassium-rich sinter.

It can be seen in Figure 5 that the sinter without enriched potassium vapor expressed three recognizable diffraction peaks: Fe_2O_3 , Fe_3O_4 , and $\text{Ca}_5\text{Si}_2(\text{FeAl})_{18}\text{O}_{36}$ (SFCA). The content of K^+ in the sinter without enriched potassium vapor is lower than the detection level of XRD, so the related phase of potassium cannot be identified. The diffraction peaks of Fe_2O_3 , Fe_3O_4 , K_2CO_3 , and KFeO_2 were found in the sinter enriched with potassium vapor. With the addition of potassium vapor, the new phases of K_2CO_3 and KFeO_2 showed recognizable diffraction peaks. K_2CO_3 resulted from the reaction (8), and KFeO_2 was formed by the reaction (9). The ΔG° -T of Equations (8) and (9) are shown in Figure 6. As can be seen from Figure 6, ΔG° of Equations (8) and (9) are both less than 0 at 500 °C, and from a thermodynamic perspective, the reactions are feasible.

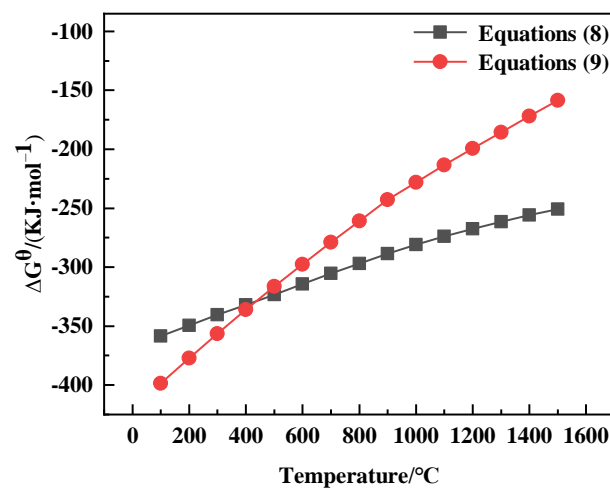


Figure 6. The ΔG° -T diagram of Equations (8) and (9).

With the addition of potassium vapor, the intensity of diffraction peaks of K_2CO_3 , $KFeO_2$, and Fe_3O_4 increased gradually, while that of Fe_2O_3 decreased gradually. Since potassium vapor reacts with CO_2 to produce K_2CO_3 , potassium vapor will react with Fe_3O_4 and CO_2 to produce $KFeO_2$ when entering the sinter, resulting in increasing contents of K_2CO_3 and $KFeO_2$. At the same time, the content of Fe_3O_4 decreased as alkali metals catalyzed the reduction reaction. When the content of potassium vapor exceeded 30 times higher, the intensity of K_2CO_3 and Fe_3O_4 diffraction peaks gradually decreased, while that of $KFeO_2$ diffraction peaks increased. This is because K_2CO_3 is mainly adsorbed on the sinter surface, and the content of potassium vapor increases. The K_2CO_3 adsorbed on the surface gradually saturates, so more potassium vapor enters the sinter and then reacts with Fe_3O_4 to produce $KFeO_2$. The content of K_2CO_3 and Fe_3O_4 decreased, while the content of $KFeO_2$ increased.

3.3.2. Microstructure Evolution and Element distributions

Figure 7 shows the SEM image and EDS spectrum of the sinter with different potassium vapor content (0, 30 times, and 50 times).

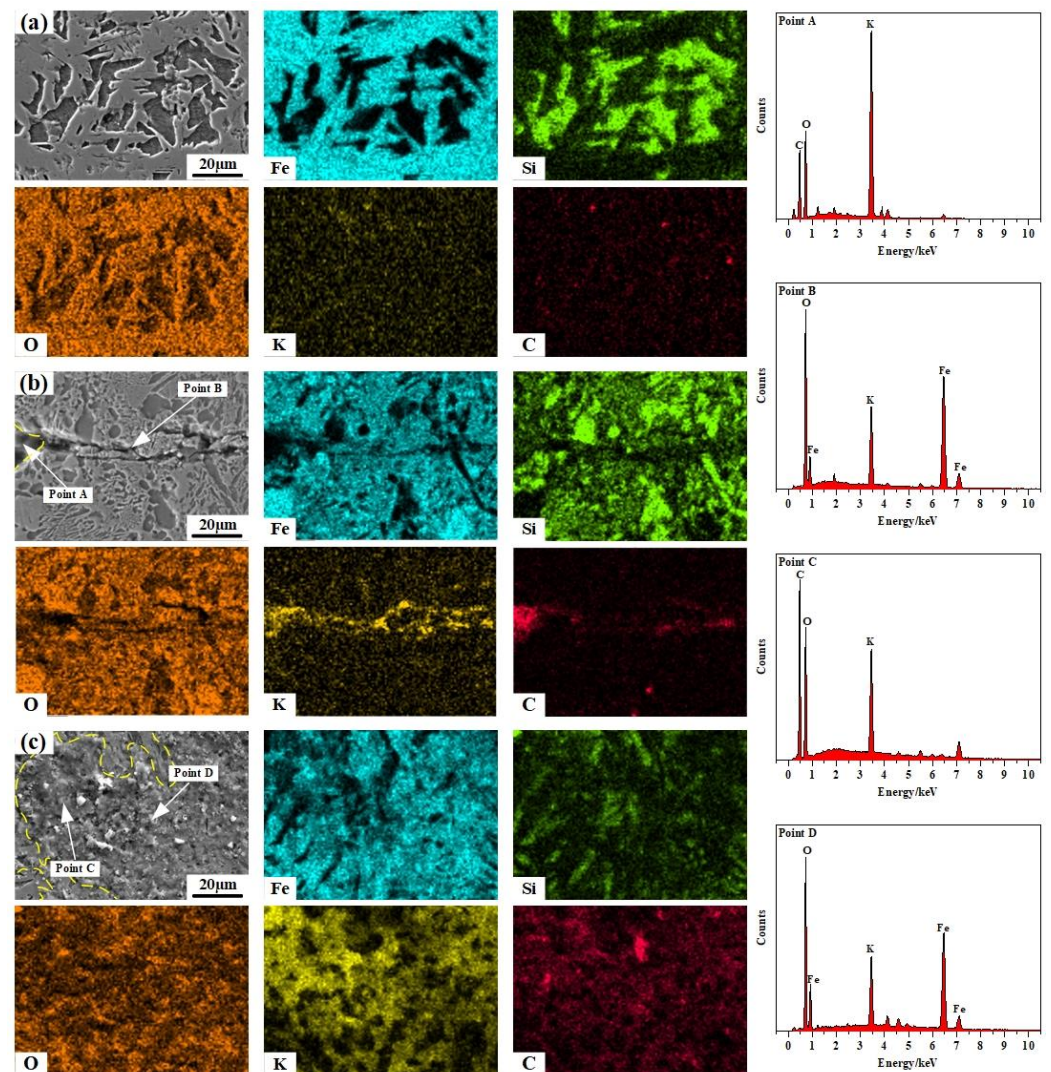


Figure 7. SEM image and EDS analysis of different potassium-rich sinter samples. (a) K-0; (b) K-30; (c) K-50.

Figure 7a shows that during the process of sintering without potassium vapor, the potassium element is lesser and evenly distributed. It can be seen from Figure 7b that when potassium vapor content is 20 times higher, inward expanding cracks appear at the edge of the sinter. Through EDS analysis, it was found that the cracks were mainly composed of Fe, O, C, and K elements. It can be seen from Figure 7c that when potassium vapor content is 50 times higher, the cross-section of the sinter has an obvious “enrichment layer”. Combined with EDS analysis, it was found that the enrichment layer was mainly composed of Fe, O, C, K, and other elements.

This is because potassium vapor is not only adsorbed on the sinter cross-section in the form of K_2CO_3 but also diffused into the sinter and combined with the surrounding hematite to form potassium ferrite. The formation of potassium ferrite consumed part of the hematite, which led to the weakening and deformation of hematite crystals, accelerated interfacial reaction rate, inhibition of the development and movement of grain connections, and production of obvious cracks. The integrity of the sinter is damaged. With the continuous increase of potassium vapor content, the content of potassic substances on the cross-section of the sinter will hinder the reduction reaction, and the distribution of potassium ferrite gradually become uniform, which is conducive to the reduction degradation performance of the sinter. The experimental results are consistent with the characteristic that the reduction degradation index of the sinter changes with the increase of potassium vapor content.

3.4. Transformation of Potassium Vapor Enrichment Form on Sinter

During the process of blast furnace ironmaking, the potassium vapor produced by the reaction in the high-temperature zone will not be completely adsorbed on the charge, part of the potassium vapor will rise with the gas, and the temperature and gas composition will gradually change. Therefore, it is necessary to determine the enrichment form transformation of potassium vapor on the sinter during the process of rising with gas. The transformation process of potassium vapor enrichment form in a sinter was simulated. Figures 8–10 show the SEM image and EDS spectra of the sinter at different reduction temperatures (1200, 1000, 800, 600, and 400 °C).

From Figure 8a,b, it can be seen that when the reduction temperature is 1200 °C and 1000 °C, large cracks appear in the dark area on the sinter surface. Combined with SEM-EDS analysis, it was found that the cracks were mainly composed of $KAlSiO_3$ and K_2SiO_3 . Y. Andou et al. took SiO_2 , Al_2O_3 , and K_2CO_3 as raw materials and found that $KAlSiO_4$ was generated at about 1000 °C, and the crystallinity increased with the increase in temperature [32]. Therefore, it can be concluded that potassium vapor reacts with aluminosilicates in the sinter to form $KAlSiO_4$ above 1000 °C. K_2SiO_3 is formed by the reaction of potassium vapor with FeO and SiO_2 in the process of sintering. The formation of $KAlSiO_4$ and K_2SiO_3 will cause lattice expansion, leading to cracks. Potassium vapor reacts with Fe_3O_4 and CO_2 to produce $KFeO_2$. At 1000–1200 °C, the Fe phase mainly exists in the form of FeO in the sinter, and the generation of $KFeO_2$ is low. At 1200 °C and 1000 °C, the potassium-containing phases of the sinter are $KAlSiO_3$, K_2SiO_3 , and a little $KFeO_2$.

Figure 9 shows that when the reduction temperature is 800 °C, a large number of white granular morphology appears, and EDS analysis indicates that the main elements in this region are Fe, K, Cl, and O. Potassium vapor can react with CO to form K_2O , which can be adsorbed on the sinter. K_2O reacts with $FeCl_2$ in the sinter to produce KCl. $KFeO_2$ and K_2CO_3 exist at the same time. Potassium vapor may also react with CO_2 to form K_2CO_3 , but K_2CO_3 is unstable and is reduced to potassium vapor. When the temperature exceeds 800 °C, the formation of K_2O is relatively difficult. Even if it is produced, SiO_2 will immediately combine into K_2SiO_3 . Therefore, the potassium-containing phases of the sinter are KCl, K_2SiO_3 , and $KFeO_2$ at 800 °C.

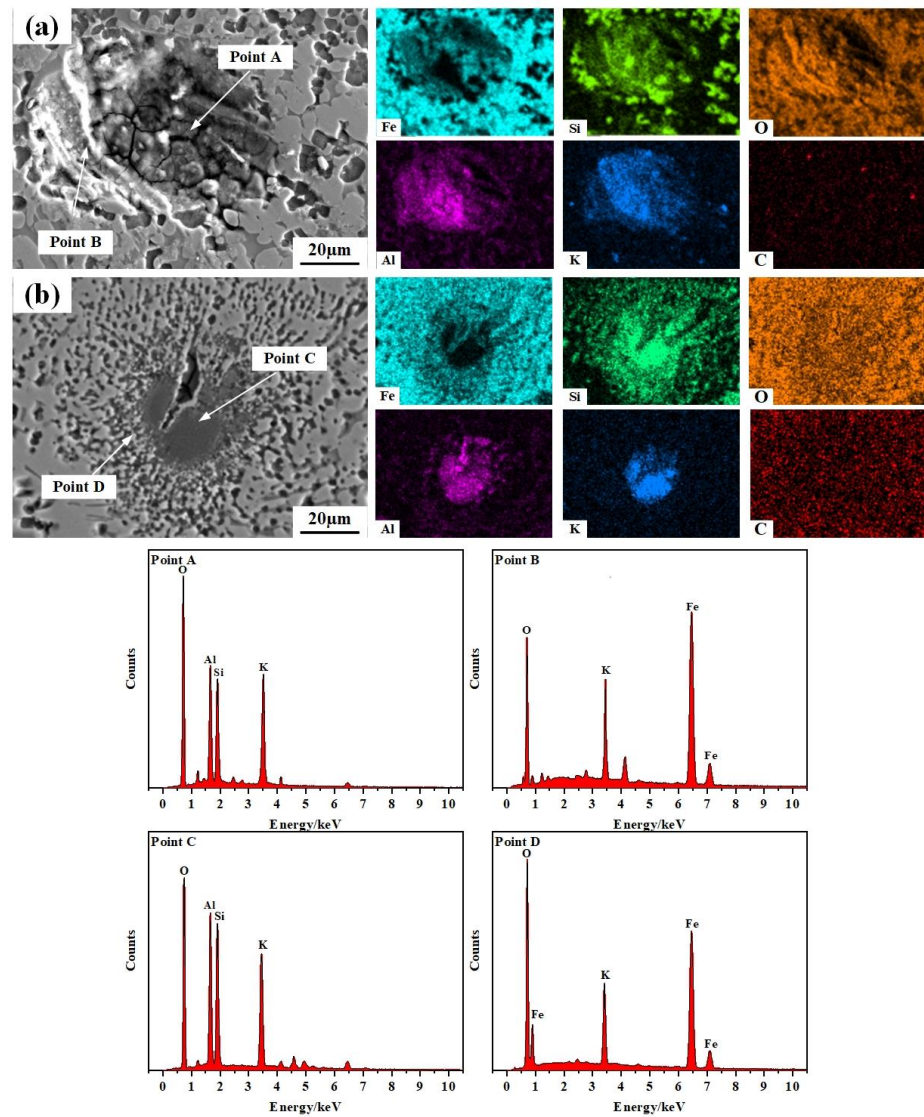


Figure 8. SEM-EDS diagram of sinter at different temperatures. (a) 1200 °C; (b) 1000 °C.

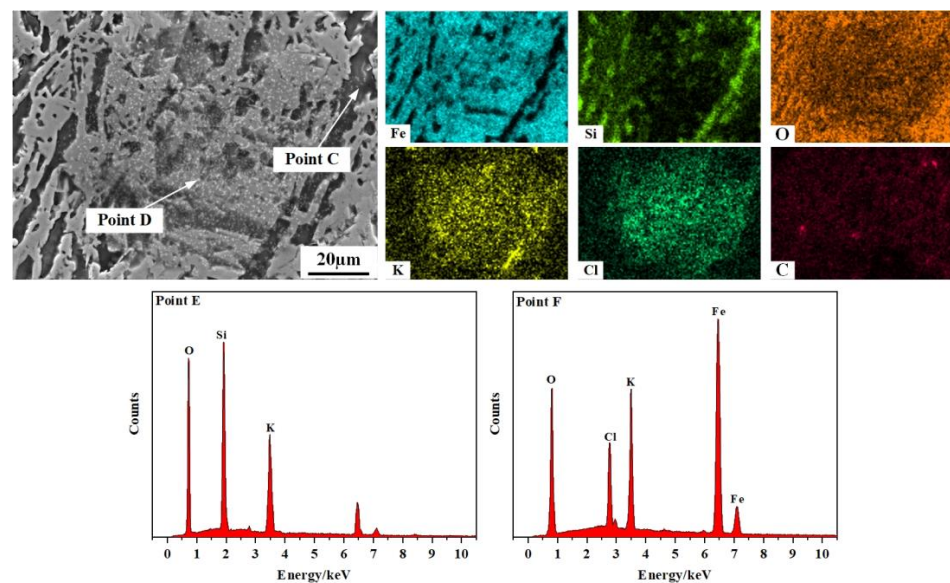


Figure 9. SEM-EDS diagram of sinter at 800 °C.

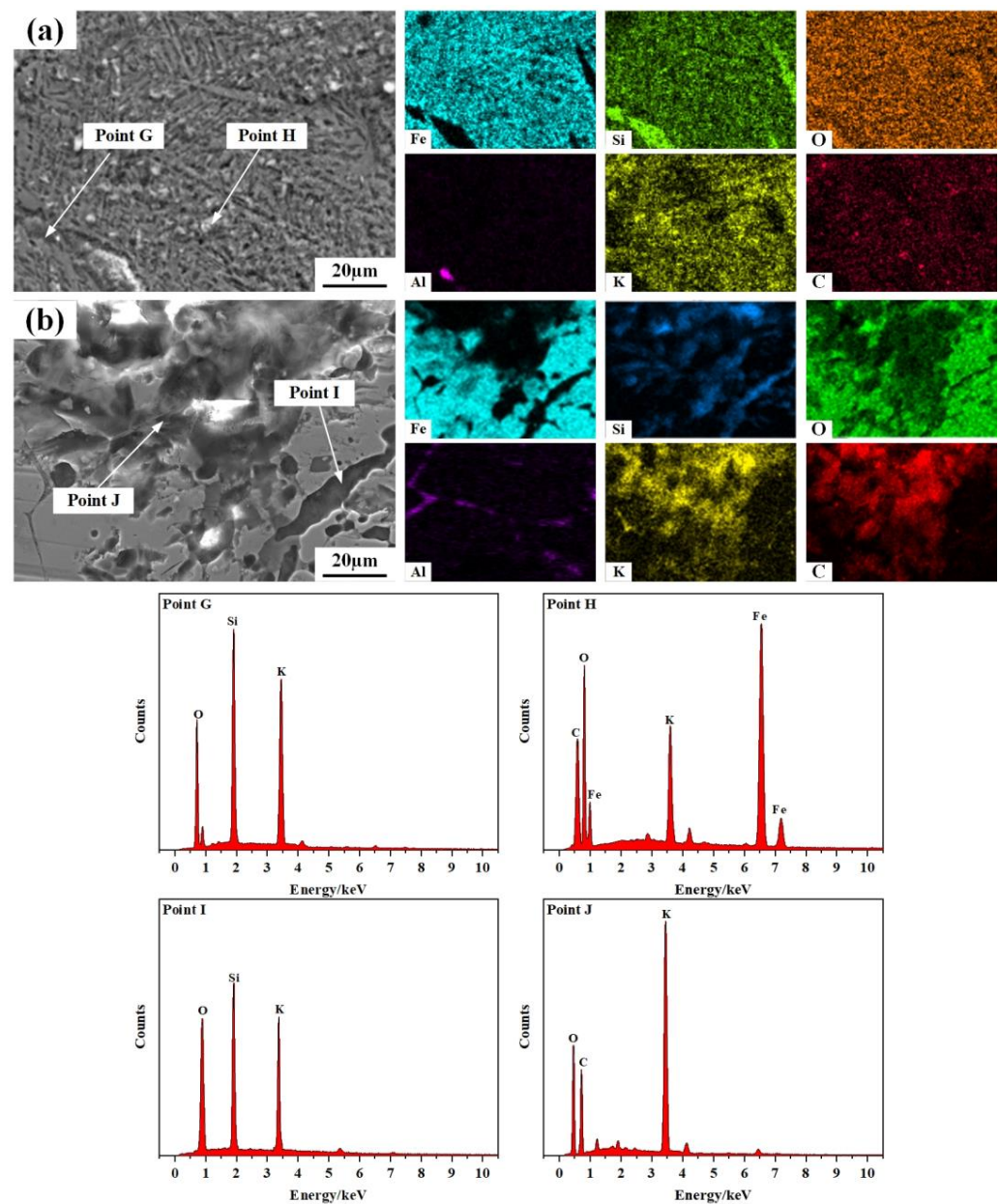


Figure 10. SEM-EDS diagram of sinter at different temperatures. (a) 600 °C; (b) 400 °C.

From Figure 10a,b, it can be seen that when the reduction temperature is 600 °C, a large number of flocculant substances exist on the surface of the sinter. Combined with SEM-EDS analysis, the elements K, Fe, C, and O of these flocculant substances were mainly found. The decrease in the reaction temperature is conducive to the formation and stability of K_2CO_3 . When the reduction temperature was 400 °C, gray matter diffused from outside to inside and appeared in the sinter. Combined with SEM-EDS analysis, the main elements K, C, and O of this gray matter were found. This is because the reduction of the reaction temperature is conducive to the formation and stability of K_2CO_3 . Meanwhile, the Fe phases in the sinter are mainly Fe_2O_3 and Fe_3O_4 at 400–600 °C and the FeO content is low, so the ability to generate $KFeO_2$ is enhanced while the ability to generate K_2SiO_3 is weak. However, when the reduction temperature is 400 °C, it is not conducive to the formation of $KFeO_2$. Therefore, the potassium phase of the sinter is K_2CO_3 , $KFeO_2$, and a small amount of K_2SiO_3 at 600 °C, and the main phase of the sinter is K_2CO_3 and a small amount of K_2SiO_3 at 400 °C.

4. Conclusions

In this paper, the occurrence form of potassium vapor in sinter and its effect on reduction degradation indexes has been studied, and the conclusions are as follows:

- (1) With the increase in potassium vapor content, the adsorption rate of potassium in the sinter first increases and then decreases. When the content of potassium vapor content is 50 times higher, the enrichment ratio of K is 2576%, and the adsorption rate of potassium is the lowest, which is 51.5%.
- (2) The main methods of potassium vapor adsorption by sinter are physical adsorption and chemical adsorption. When the potassium vapor content is less than 30 times higher, the potassium vapor is mainly adsorbed on the sinter surface in the form of K_2CO_3 , while the potassium vapor diffuses to the sinter and reacts with Fe_3O_4 to form $KFeO_2$, which results in the decrease of $RDI_{+3.15mm}$. With the continuous increase of potassium vapor content, the $KFeO_2$ distribution is uniform, and the $RDI_{+3.15mm}$ improves.
- (3) In the process of potassium vapor rising with gas, at 1200 °C and 1000 °C, potassium vapor mainly exists in the sinter in the form of $KAlSiO_3$ and K_2SiO_3 . At 800 °C, the potassic phases of the sinter are KCl , K_2SiO_3 , and $KFeO_2$. At 600 °C, potassium vapor mainly exists in the form of K_2CO_3 , K_2SiO_3 , and $KFeO_2$. At 400 °C, potassium vapor is mainly adsorbed on the sinter in the form of K_2CO_3 .

Author Contributions: Conceptualization, J.J., H.W. and X.X.; methodology, J.J.; software, M.L.; validation, M.L.; formal analysis, H.W. and X.X.; investigation, J.J., H.W. and X.X.; resources, J.J. and H.W.; data curation, M.L.; writing—original draft preparation, J.J., H.W. and X.X.; writing—review and editing, J.J., H.W. and X.X.; visualization, M.L., G.Z. and X.J.; supervision, X.X., M.L., G.Z. and X.J.; funding acquisition, G.Z. and X.J. All authors have read and agreed to the published version of the manuscript.

Funding: The present work was financially supported by the Natural Science Basic Foundation of China (Program No. 52174325), the Key Research and Development Project of Shaanxi Province (Grant No. 2019TSLGY05-05) and the Shaanxi Provincial Innovation Capacity Support Plan (Grant No. 2023-CX-TD-53). The authors gratefully acknowledge their support.

Data Availability Statement: Some data has been provided in the article. If necessary, you can contact the author.

Acknowledgments: The assistance and resources provided by Xi'an University of Architecture and Technology and the Technology Center of Jiuquan Iron & Steel (Group) Co., Ltd. made it possible for us to complete this study. We are grateful to them for their help.

Conflicts of Interest: The authors declare no conflict of interest.

References

1. Cai, C.Q.; Su, X.C.; Huang, B. Recycling of dust removal ash in iron and steel production process. *China Met. Bull.* **2022**, *1074*, 102–104.
2. Wang, C.H.; Jiang, X.T. Property analysis and utilization technology of dust ash in Jiusteel. *Metallurgy* **2019**, *29*, 57–62.
3. Lanzerstorfer, C.; Bamberger-Strassmayr, B.; Pilz, K. Recycling of blast furnace dust in the iron ore sintering process: Investigation of coke breeze substitution and the influence on off-gas emissions. *ISIJ Int.* **2015**, *55*, 758–764. [[CrossRef](#)]
4. Zhao, Y.M.; Feng, C.Y.; Li, D.X. The Major Ore Clusters of Super-Large Iron Deposits in the World, Present Situation of Iron Resources in China and Prospect. *Acta Geol. Sin. Engl. Ed.* **2014**, *88*, 1895–1915. [[CrossRef](#)]
5. Kurunov, L.F.; Titov, V.N.; Emel'yanov, V.L. Analysis of the behavior of alkalis in a blast furnace. *Metallurgist* **2009**, *53*, 9–10. [[CrossRef](#)]
6. Gridasov, V.P.; Logachev, G.N.; Pishnograev, S.N. Behavior of Alkalis in Blast Furnaces. *Metallurgist* **2016**, *59*, 9–10. [[CrossRef](#)]
7. Zhao, H.; Cheng, S. New cognition on coke degradation by potassium and sodium in alkali enriched regions and quantificational control model for BF. *J. Univ. Sci. Technol. Beijing* **2012**, *34*, 333–341.
8. Hilding, T.; Gupta, S.; Sahajwalla, V. Degradation behaviour of a high CSR coke in an experimental blast furnace: Effect of carbon structure and alkali reactions. *ISIJ Int.* **2005**, *45*, 1041–1050. [[CrossRef](#)]
9. Wang, M.C.; Wei, G.S.; Yang, S.F. Effect of alkali (K/Na) metal vapor on the metallurgical properties of coke in CO_2 – O_2 – N_2 mixed atmosphere. *Energy* **2022**, *257*, 124748–124763. [[CrossRef](#)]

10. Wang, G.W.; Ren, S.; Zhang, J.L. Influence mechanism of alkali metals on CO₂ gasification properties of metallurgical coke. *Chem. Eng. J.* **2020**, *387*, 124093–124106. [[CrossRef](#)]
11. Wang, Y.B.; Luo, G.P. Effect of MgO, fluorine and alkali metals on mineral phase of pellets. *Iron Steel* **2022**, *57*, 34–42.
12. Wang, S.J.; Wang, W.; Chen, R.G. Research on effect of potassium on metallurgical properties of pellets. *Sintered Pellet* **2021**, *46*, 44–49.
13. Wang, Z.X.; Feng, S.; Wang, Y.L. Influence on blast furnace burden by alkali metals. *Sichuan Metall.* **2020**, *42*, 29–32.
14. Fang, M.X.; Hou, X.J.; Hou, Z.Y. Alkali vapor corrosion of refractories at high temperatures. *Refractories* **2021**, *55*, 296–301.
15. Jiao, K.X.; Zhang, J.L.; Liu, Z.J. Analysis of Blast Furnace Hearth Sidewall Erosion and Protective Layer Formation. *ISIJ Int.* **2016**, *56*, 1956–1963. [[CrossRef](#)]
16. Jin, Y.L.; He, Z.J.; Wang, C. Analysis on low carbon emission of blast furnace with different raw materials structure. *Iron Steel* **2019**, *54*, 8–16.
17. Zhou, D.D.; Cheng, S.S.; Wang, Y.S. The production of large blast furnaces during 2016 and future development of ironmaking in China. *Ironmak. Steelmak.* **2017**, *44*, 714–720. [[CrossRef](#)]
18. Bahgat, M.; Halim, K.S.A.; El-Kelesh, H.A. Metallic iron whisker formation and growth during iron oxide reduction: K₂O effect. *Ironmak. Steelmak.* **2019**, *36*, 379–387. [[CrossRef](#)]
19. Zhang, X.; Jiang, X.; Wang, X.B. Experimental study on influence of K₂O on strength of sinter. *Iron Steel* **2020**, *55*, 49–55.
20. Yan, Z.L.; Li, X.Y.; Liu, Z.J. Study on influence of gas phase potassium adsorption on metallurgical properties of sinter. *J. Sintered Pellets* **2016**, *9*, 1–5, discussion 31.
21. Kang, Z.P.; Li, J.C.; Si, J.C. Effect of harmful trace elements on metallurgical properties of blast furnace burden in Hansteel. *Iron Steel Res.* **2014**, *42*, 10–12, discussion 15.
22. Wang, X.Z.; Yan, Z.W.; Wang, R.R. Study of the enrichment characteristics of sinter by alkali metal vapors. *Metall. Res. Technol.* **2018**, *115*, 310–319. [[CrossRef](#)]
23. Cheng, G.J. Study on Kinetics of High Chromia Vanadium-Titanium Magnetite Reduction and Migration Behavior of Valuable Elements in Lumpy Zone. Master's Thesis, Northeastern University, Liaoning, China, 2013.
24. Li, P.; Liu, W.; Zhang, H.X. Impact of Potassium on Gasification Reaction and Post-Reaction Strength of Ferro-coke. *ISIJ Int.* **2017**, *57*, 1947–1954. [[CrossRef](#)]
25. Fan, X.Y. Study on the Formation and Evolution of the Slag Phase in the Cohesive Zone of the Blast Furnace. Ph.D. Thesis, Beijing University of Science and Technology, Beijing, China, 2022.
26. Chen, S.P.; Wang, W.; Xu, R.S. Influence of multiple factors on the alkali metal enrichment in blast furnaces by a thermodynamic model. *Ironmak. Steelmak.* **2020**, *47*, 219–227. [[CrossRef](#)]
27. Li, K.J.; Zhang, J.L.; Barati, M. Influence of alkaline (Na, K) vapors on carbon and mineral behavior in blast furnace cokes. *Fuel* **2015**, *145*, 202–213. [[CrossRef](#)]
28. Zhu, B.; Zhou, J.D.; Zhao, L.C. Occurrence form of zinc in blast furnace and its influence on sinter performance. *Iron Steel* **2020**, *55*, 130–139.
29. Zhu, B.; Zhou, J.D.; Pan, Y. Study on enrichment and occurrence form of zinc on coke in upper part of blast furnace. *J. Iron Steel Res.* **2020**, *32*, 690–699.
30. GB/T 6730.49-2017; Iron Ores Determination of Potassium Content Flame Atomic Absorption Spectrometric Method. General Administration of Quality Supervision, Inspection and Quarantine of China: Beijing, China, 2017.
31. GB/T 13241-2017; Iron Ores Determination of Reducibility. General Administration of Quality Supervision, Inspection and Quarantine of China: Beijing, China, 2017.
32. Andou, Y.; Kawahara, A. The refinement of the structure of synthetic kalsilite. *Mineral. J.* **1984**, *12*, 153–161. [[CrossRef](#)]

Disclaimer/Publisher's Note: The statements, opinions and data contained in all publications are solely those of the individual author(s) and contributor(s) and not of MDPI and/or the editor(s). MDPI and/or the editor(s) disclaim responsibility for any injury to people or property resulting from any ideas, methods, instructions or products referred to in the content.